LASER
& PHOTONICS
REVIEWS

Laser Photonics Rev. **9,** No. 4, 392–398 (2015) / **DOI** 10.1002/lpor.201400462

ORIGINAL
PAPER

Abstract Recent realization of nontrivial topological phases in photonic systems has provided unprecedented opportunities in steering light flow in novel manners. Based on the Su–Schriffer–Heeger (SSH) model, a topologically protected optical mode was successfully demonstrated in a plasmonic waveguide array with a kinked interface that exhibits a robust nonspreading feature. However, under the same excitation conditions, another antikinked structure seemingly cannot support such a topological interface mode, which appears to be inconsistent with the SSH model. Theoretical calculations are carried out based on the coupled-mode theory, in which the mode properties, excitation conditions, and the robustness are studied in detail. It is revealed that under the exact eigenstate excitations, both kinked and antikinked structures do support such robust topological interface modes; however, for a realistic single-waveguide input only the kinked structure does so. It is concluded that the symmetry of interface eigenmodes plays a crucial role, and the odd eigenmode in a kinked structure offers the capacity to excite the nonspreading interface mode in the realistic excitation of a one-waveguide input. Our finding deepens the understanding of mode excitation and propagation in coupled waveguide systems, and could open a new avenue in optical simulations and photonic designs.

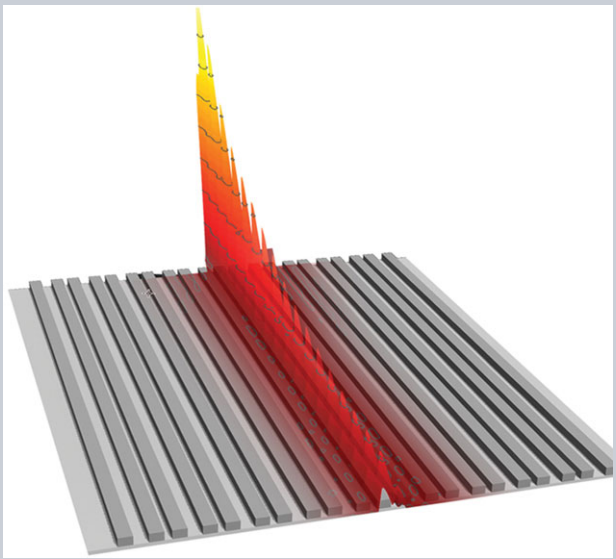

Topologically protected interface mode in plasmonic waveguide arrays

Qingqing Cheng, Yiming Pan**, Qianjin Wang, Tao Li*, and Shining Zhu**

1. Introduction

Topological phases have opened up a fascinating avenue in modern physics with manifestations of striking phenomena, such as the quantum Hall effect [1], and topological insulators [1–3]. As a successful extension to the optical system, the photonic edge state, a nontrivial topological phase [4, 5], gives rise to novel one-way optical propagations and robustness against scattering from defects, which have been well demonstrated in two-dimensional (2D) photonic crystals [6–8]. Besides the attractive 2D band structures, another intriguing exploration is in the 1D topological systems, such as solitons [9] and Majorana fermions [10]. Fortunately, the Su–Schriffer–Heeger (SSH) model revealed in polyacetylene [9] is one of the most interesting 1D topological structures, which has two topologically inequivalent phases according to its different dimerization patterns [11]. Induced by the presence of the kinked defects [11], correspondingly, a topologically protected zero-dimensional edge state appears at the interface, which acts as a moving domain wall with nontrivial Berry phase (or Zak phase) [3, 12, 13]. Indeed, the soliton and Majorana fermion are two fundamental topological zero modes in condensed-matter physics. The optical mimics of the SSH model were investigated in optical lattices [11, 15], quantum walks [14] and the coupled microwave resonators [16]. Recently, a simulation of Majorana fermions was realized on a 1D zigzag array of plasmonic nanoparticles that mimics the Kitaev model by mapping the particle–hole excitation into polarization-degeneration of plasmonic modes [17]. However, the light diffraction in a waveguide array, as an important simulator for condensed-matter physics [18, 19], has not yet been demonstrated in a 1D topological system.

In the optical regime, metallic waveguide arrays [20,21] and layered metamaterials [22], based on the coupling of surface plasmonic polaritons (SPPs), have drawn much attention owing to not only the strong field confinement [20] but also their controllability in diffraction management [22, 23]. Compared with the dielectric ones [19], the plasmonic waveguide array (PWA) offers a much wider coupling range and even to the anomalous region (i.e., negative coupling coefficient) for its particular field configurations [20,22], which have already shown many interesting optical

National Laboratory of Solid State Microstructures, College of Engineering and Applied Sciences, School of Physics, Collaborative Innovation Center of Advanced Microstructures, Nanjing University, Nanjing 210093, China
**These authors contributed equally to this work.
*Corresponding author: e-mail: taoli@nju.edu.cn

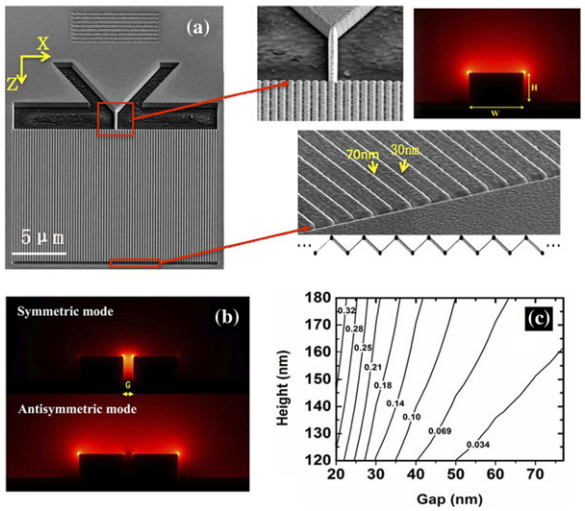

Figure 1 (a) SEM image of experimental sample including grating, funnel-shaped coupled-in, and ridge waveguides array ($N = 79$), where the mode distribution of a single-ridge waveguide is presented. (b) Simulated electric-field intensity distributions of symmetric and antisymmetric modes on the two coupled ridge waveguides. (c) Contour map of coupling coefficient as a function of the PWAs height and gap at a fixed PWA width of 300 nm ($\lambda = 633$ nm).

properties (e.g., negative refraction [21, 23]) and quantum-optical analogies (e.g., Bloch oscillations [24] and surface modes [25, 26]). Since the robustness of the interface state in SSH have been revealed in several systems [12, 14, 16], a topologically protected SPP propagation would be highly expected.

In this paper, we proposed and demonstrated, for the first time, a topologically protected plasmonic interface mode in a metallic ridge waveguide array. Though the SSH model predicted that there are two kinds of interface states with topological protection, our experimental results seemingly show that only one (the kinked) does so. To obtain an insightful understanding into this unusual phenomenon, we investigate the SPP propagations in PWAs with two kinds of defects in detail by the coupled-mode theory (CMT), where the influence of excitation conditions, loss and robustness are discussed. Finally, we find that in an ideal lossless system the eigeninterface states would be topologically protected in both structures, but in a real system only the kinked structure is achievable in an available condition of optical excitation. Our finding deepens the understanding of confinement and diffraction of SPPs in a coupled waveguide array, and could illuminate informative simulations for the topological systems in condensed-matter physics.

2. Modeling of plasmonic waveguide array

Metallic ridge waveguides are introduced to model the PWAs, which would be conveniently achieved experimentally by current nanofabrication (see Fig. 1). According to the notation of Su, Schriffer, and Heeger (SSH), a perfect dimer chain of polyacetylene has two degenerated ground states – phases A and B, which correspond to the *sublattice symmetry* (i.e., chiral symmetry [9,11]) with alternating double bonds and single bonds. When chains with these two phases are connected together, there will be two kinds of topological excitations with respect to two different connections (kinked and antikinked), which are also described as the domain walls between phases A and B. The SSH model has already revealed a unique feature of solitary waves, termed a "topological soliton or antisoliton" [11]. Following the coupled-mode theory (CMT), the field propagation of SPP within the PWA can be described by

$$-i\frac{\partial}{\partial z}a_j = \beta_j a_j + \kappa_{j,j+1}a_{j+1} + \kappa_{j,j-1}a_{j-1} \qquad (1)$$

analogous to the tight-binding approximation (TBA) model [24], where a_j is the amplitude of the plasmonic field in the jth ridge waveguide (here $j = -39, -38, \ldots, 38, 39$ according to our experimental sample of $N = 79$), κ is the coupling coefficient between the neighboring waveguides. Based on a commercial FEM solution (Comsol Multiphysics 4.3a, see the Supporting Information), the mode property and effective propagation constant is simulated for a single silver ridge waveguide with a width of 300 nm and a height of 150 nm at the wavelength $\lambda = 633$ nm. From the simulation, it is obvious that the ridge plasmonic mode has an electric field tightly confined on the surface and corners of the ridge (see Fig. 1a). When two waveguides are close enough, plasmonic modes will be coupled with a coefficient of $\kappa_{n,n+1}$ between the nth waveguide and the $(n+1)$th waveguide in the array, which gives rise to the symmetric (β_s) and antisymmetric (β_a) modes, as shown in Fig. 1b. The coupling coefficient can be defined by $\kappa_{n,n+1} = (\beta_s - \beta_a)/2$ [21, 22], which was systematically investigated according to a series of structural parameters. Figure 1c shows a contour diagram of the coupling coefficient κ (from 0.034 to 0.32) with respect to a certain range of structure parameters (height from 120 nm to 180 nm, gap from 20 nm to 80 nm, and a fixed ridge width of 300 nm). This wide range of κ offers us a free selection in PWA designs with two different coupling strengths to simulate the SSH model.

3. Sample fabrication and experimental results

The experimental sample was designed on a silver film (thickness about 300 nm), which includes the grating, funnel-shaped coupled-in, and the array of 79 plasmonic waveguides (see Fig. 1a). In nanofabrication, a silver film was sputtered on a quartz substrate and followed with focused ion beam (Dual Beam Helios 600*i*) milling to fabricate gratings, PWAs and funnel-shaped structures. According to simulation results, the ridge waveguide is designed with a width of 300 nm and a height of 150 nm (corresponding to a mode index of $\beta_n = 1.047k_0$ with an imaginary part of $\sim 0.0017k_0$), and the alternating gaps are 30 nm and

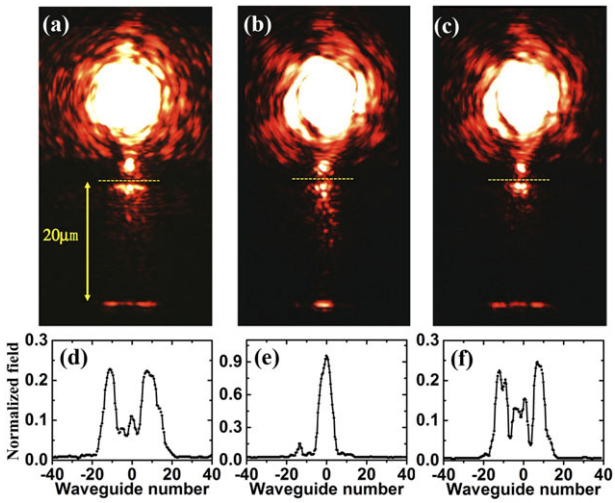

Figure 2 (a–c) CCD recorded field intensities for the PWA-S0, S1 and S2, respectively. (d–f) Normalized intensity profiles at the ends of PWAs corresponding to the three samples, which clearly reflect different diffractions and of SPPs in different PWAs: normal diffraction of the binary periodic waveguide array (PWA-S0), strongly localized at the domain wall in the kinked sample (S1), and a mixed feature of localization and spreading in the antikinked one (S2).

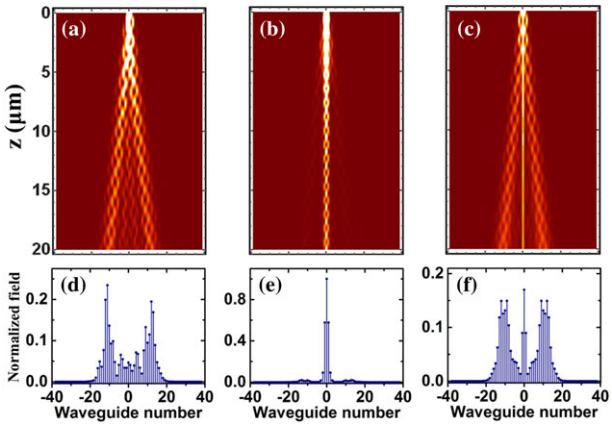

Figure 3 (a–c) CMT calculated SPP intensities in propagations for PWA-S0, S1, and S2, respectively. (d–f) Field intensity subtracted from the output with a distance of 20 μm. It is clearly shown that PWA-S0 has a normal diffraction, S1 exhibits a strong localized mode within the center interface, while S2 displays a mixed feature.

70 nm, corresponding to $\kappa_1 = 0.188$ (Im(κ_1)~0.0048) and $\kappa_2 = 0.034$ (Im(κ_2)~0.0021), respectively, with the units of k_0 (the imaginary parts of β and κ being obtained by the mode analyses via COMSOL simulations). In the center of the array, two kinds of defects are formed by two strong couplings (gap of 30 nm) and two weak couplings (gap of 70 nm) termed kink and antikink, respectively. For convenience, we define the kinked sample as PWA-S1 and the antikinked one as PWA-S2 (see the top insets in Fig. 4). A defectless SSH sample PWA-S0 was also investigated for comparisons. In optical analyses, a transverse magnetically (TM) polarized He-Ne laser (633 nm) was coupled to a planar SPP mode by the grating, and then converted to ridge SPP to excite the central defect mode of the PWA via the funnel structure. The propagation information will be detected by the scattering field from the end of the array, which can be directly imaged by a microscope.

Figures 2a–c clearly show different SPP propagations in three samples (PWA-S0, S1 and S2), and the corresponding scattered field profiles are depicted in Figs. 2d–f, respectively. It is evident that the PWA-S0, as a reference, exhibits two well-separated peaks at about the $\pm$10th waveguide in the intensity profile, corresponding to a normal dispersive diffraction in a binary periodic waveguide array [21, 23]. However, PWA-S1 with the kinked defect (strong coupled) demonstrates a strong localized intensity peak at the center of the waveguide array, indicating a confined interface mode. This is consistent with the topological SSH model, as expected [14]. Being checked in other samples with waveguide length different from 20 μm (e.g., 15 μm), this localized mode is repeated, which strongly manifests a well-achieved plasmonic interface mode (see Fig. S1 and Fig. S2 in the Supporting Information). Surprisingly, another sample (PWA-S2) shows an obvious field spreading, though a weak-intensity peak still remains at the center. This phenomenon apparently contradicts with what the SSH model predicts.

4. Theoretical calculations and analyses

In order to confirm the experiments and reveal the underlying physics of the distinct behaviors of SPP propagations in these two PWAs, we performed theoretical calculations based on the CMT (see Eq. (1)). Although the input of SPP is from a single waveguide in experiments, the evanescent field would possibly spread to a certain spatial area and two neighboring waveguides would be partially excited. Since the CMT calculation only allows the definition of the field within every lattice (waveguide), it is reasonable to define the single-waveguide input as a wavepacket excitation that covers three waveguides with a certain intensity ratio (0.5/1/0.5, approximately). Figure 3 shows the calculation results of three samples (PWA-S0, S1, and S2), where the alternating coupling coefficients are set as $\kappa = 0.188$ and 0.034 with their imaginary parts included, corresponding to the gaps of 30 nm and 70 nm, respectively. The output intensities extracted from the distance of 20 μm show good agreement with the experimental result. It is evident that the S1 exhibits a strong localized peak, while a mixed feature of localization and strong dispersive is revealed in S2.

Unfortunately, the theoretical results did not yet answer the question as to why the PWA-S2 sample is inconsistent with the SSH model. To produce an indepth understanding of this interesting phenomenon, we are going to analyze the eigenmodes of two kinked structures in detail. Here, we rewrite the coupled-mode equations into the Schrödinger type with only the real values of β and κ, and solve the eigenvalues problem of the corresponding Hamiltonians

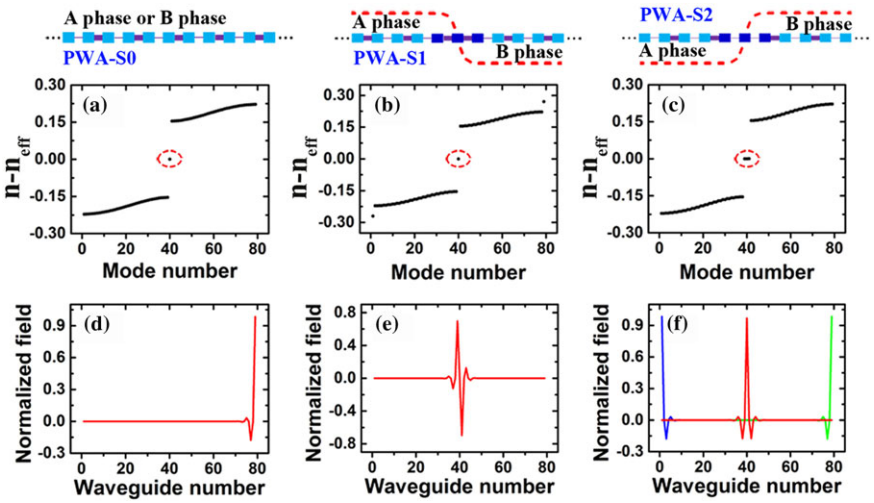

Figure 4 (a–c) Mode diagrams with zero modes circled for PWA-S0, S1, and S2, respectively; (d–f) Field distributions of the zero-energy modes, showing quite different properties. The zero mode is strongly localized at the right boundary with a suspended single bond for S0 (while the suspended double bond at the left boundary does not support this edge mode). The zero mode in S1 corresponds to a localization at the center interface with an odd symmetry of the field distribution. However, for S2, there are three degenerated zero modes distribute at the interface and edges, where two edge modes correspond to two suspended single bonds at the two boundaries, and the center even-symmetric mode belongs to the interface.

H_1 and H_2 of three 79 single-waveguide arrays for S1 and S2 [27] (see the Supporting Information). The calculated mode diagrams are shown in Figs. 4a–c for three samples of PWA-S0, S1 and S2, respectively, above which the waveguide configurations are schematically plotted. It is found that there are discrete modes (circled ones) with a zero-mode index (n–$n_{\text{eff}} = 0$) in the midgap termed "zero modes". Let us first look at the defectless PWA-S0. The zero-mode profile is displayed in Fig. 4d, which apparently corresponds to an edge state from a suspended single bond at the right boundary of the array (the suspended double bond at the left boundary does not support such a local mode) [27]. As for the zero mode in PWA-S1, the field distribution indicates an interface mode at the kinked domain wall (see Fig. 4e). However, for PWA-S2, three zero modes are found, whose field profiles are displayed in Fig. 4f. It is well recognized that two side modes actually belong to the edge states at two boundaries (due to suspended single bonds in this antikinked 79-waveguide array), and the center mode (the red one) should be an interface mode similar to the zero mode in PWA-S1. According to the basic property of eigenmodes, the mode profiles will not change along the propagations. This means that the zero mode, as a particular eigenmode inside the bandgap, would be robust due to protection of the bandgap that prevents its transfer into the bulk modes. However, in our theoretical calculation (see Fig. 3), we did not define the exact eigenmode as the initial conditions, which would be the clue to understand the different behaviors of S1 and S2. Therefore, the influence of the excitation conditions will be particularly investigated in the following section.

5. Influence of the excitation conditions and losses

Given the field distributions of the eigenzero modes of PWA-S1 and S2 as the initial conditions, we recalculated the SPP propagations based on the CMT within the 79-waveguide array. First, we neglect the loss of SPPs (i.e., the imaginary parts both of β and κ) according to the Hermitian SSH model. Figures 5a and e show the calculation results of PWA-S1 and S2, respectively, which demonstrate two well-confined modes within the kinked (antikinked) domain walls without spreading. This is really consistent with the definition of the eigenstates. However, in real circumstances, it is difficult to excite the PWAs with the exact eigenmode profile due to the particular phase requirement in the input process. Usually, the initial condition is set as an intensity peak at the defect region, which only covers a single or several waveguides with the same phases. So, these inphase wavepackets would be approximately considered as the amplitude profiles of the eigenzero modes. In this regard, initial conditions with only amplitude are set (see the top-inset figures) in the calculations, as shown in Figs. 5b and f, respectively. It is amazing to find that the PWA-S1 keeps a good nonspreading character with a field beating, while the PWA-S2 has a certain amount of energy spreading, revealing a mixed feature of dispersive and localization. This really indicates that the excitation condition does play an important role in the field evolution. To further uncover the secret of the different behaviors in amplitude excitations for S1 and S2, we decompose the mode profiles with respect to their eigenzero modes. Figures 5c and g show the SPP propagations excited with the resultant mode profiles by subtracting the eigenmodes from the amplitude profiles, as displayed in the top of field evolution maps. According to the odd symmetry of the eigenstate in S1, the resultant mode profile exhibits a half of the eigenmode that leads to an oscillating beaming within the kinked structure without spreading. By contrast, the resultant profile of excitation in S2 has two separated peaks that greatly deviate from the eigenmode due to the even symmetry, which reasonably spreads into the bulk modes with well-separated ballistic patterns. Thus, the distinct behaviors in the kinked and antikinked SSH PWAs arise from the phaseless excitations, which have quite different decomposition with respect to their eigenmodes. In short, the symmetry of the zero mode plays the crucial role in determining the dispersion of the defect modes.

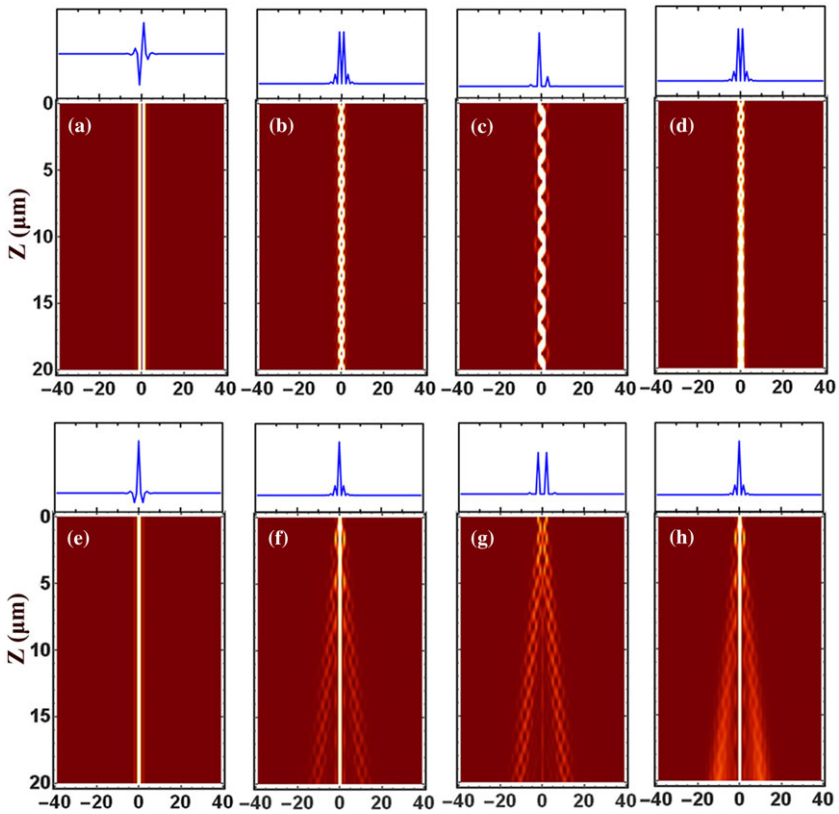

Figure 5 (a–d) CMT calculated SPP field evolution maps for PWA-S1 with excitations of (a) an exact eigenmode, (b) an amplitude profile of eigenmode, (c) a decomposed profile by subtracting the eigenmode from the amplitude one, (d) an amplitude profile with loss. (e–h) the corresponding calculation results for PWA-S2. The excitation conditions are plotted on the top of the field evolution map correspondingly.

In order to link the results of eigen- (amplitude) modes more closely to the real plasmonic system, the metallic absorption loss should be considered. It has been recently reported in a lossy coupled waveguide system that even the homogeneous absorption always influences the light dynamics [28]. Because the imaginary off-diagonal elements in the Hamiltonian cannot be removed by normalization, the presence of loss will cause deviations in light propagations. Moreover, the diffractions within the waveguide array tend to change from ballistic to diffusive (see Ref. [28] for details). Here, we added the imaginary parts of β and κ as obtained from the COMSOL simulation in the CMT calculation with respect to the amplitude input excitations, as the results shown in Figs. 5d and h. It can be seen that there is no apparent difference between the lossy and lossless ones, where S1 still keeps nonspreading and S2 has the dispersive components. More careful observations show that the beating patterns in both cases tend to be smoothed out in the lossy systems, indicating a conversion from ballistic to diffusive, which is well consistent with Ref. [28]. Also, a characteristic distance can be estimated according to Eq. (10) in Ref. [28] to be 8–9 μm, which also agrees well with the results of Figs. 5d and h. Strictly, the presence of loss changes the Hermitian SSH system to non-Hermitian, and the dispersion property would be modified due to the complex coupling. However, the propagation region that we investigated is only 20 μm, which is not much larger than the characteristic distance. Therefore, the major properties holding for the SSH model can be demonstrated via the SPP propagations in such a lossy system. Additionally, these results are in good coincidence with the simulative calculations for the experiments (Fig. 3), where the excitations are not designed as the amplitudes of eigenmodes but a single-waveguide input. This means the experimental result of S1 can be reasonably considered as the interface state excited within the kinked SSH structure.

6. Robustness against disorders

Thus, it is recognized that the symmetry of zero modes is the very cause that determines whether an discrete excitation of the PWA can lead to a nonspreading interface mode, so as to mimic the solitary wave predicted by the SSH model. It has been experimentally demonstrated that the SPP in S1 appears to be a topologically protect interface mode, but its robustness against the disorders still needs to be verified. In the following CMT calculations, we introduced structural disorder [16] by defining the coupling coefficients as $\kappa = \kappa + \frac{W}{2}\xi$, where W is the disorder strength in the units of k_0, and ξ is a random number uniformly distributed in the interval $[-1,1]$. Figures 6a–c display the calculation results for the disordered S1 sample with the exact eigenmode excitation, lossless, and lossy single-waveguide input, respectively. It is evident that the nonspreading property of the SPP propagation is almost maintained, implying the topologically protected interface state in the experiment. As for the S2, the exact eigenexcitation results in an almost unchanged localized mode (see Fig. 6d), indicating this

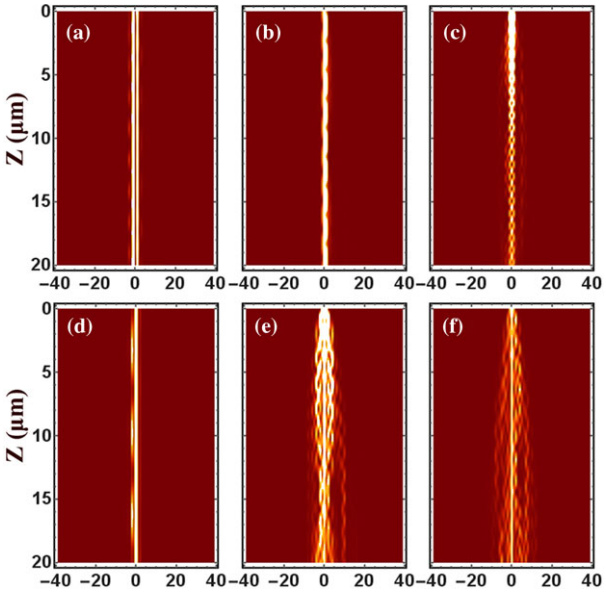

Figure 6 (a–c) CMT calulated SPP field evolution maps for the disordered PWA-S1 (disorder strength of $W = 0.188$ for strong κ_1 and 0.033 for weak κ_2) with excitations of (a) an exact eigenmode, (b) a single-waveguide input without loss, (c) a single-waveguide input with loss. (d–f) the corresponding calculation results for PWA-S2.

mode is intrinsically a topological SSH interface state that should be protected in the same way as that in S1, whereas the dispersive propagation excited by a single-waveguide input demonstrates strong disturbed propagation behaviors both for the lossless and lossy ones, as shown in Figs. 6e and f, respectively. Here, the disorder strength W is set as 0.188 and 0.033 for the strong coupling and weak coupling, respectively, corresponding to the coupling strengths.

In fact, the machining accuracy in FIB fabrication is about 10 nm in our experiments. According to the diagram of the coupling coefficient in Fig. 1c, the disorder strength deviation ΔW with the fabrication error of 10 nm is about 0.204 at the central gap of 30 nm ($\kappa_1 = 0.188$) and is about 0.029 at the central gap of 70 nm ($\kappa_2 = 0.033$), which are both comparable to the corresponding coupling coefficient and thus the manufacturing error cannot be ignored. By carefully comparing a number of samples with the same designed parameters (gap = 30 nm/70 nm), almost unchanged interface modes are observed with clear topological localized peaks in PWA-S1 (see Fig. 7a) that agrees well with the calculations (Fig. 6c), clearly showing the immunity against the manufacturing errors. However, in the same circumstances, the PWA-S2 sample exhibits randomly various output distributions (see Fig. 7b) that well confirm the loss of the topological protection.

6. Conclusion

In conclusion, we presented the first systematic study on the SSH model in SPP waveguide arrays with respect to two types of kinked structures. It was revealed in experiments that the kinked structure supports a topologically protected interface mode with immunity to structure disorders, while the antikinked one does not. Our detailed and indepth study provided a sound explanation on this interesting phenomenon that the excitation condition plays a major role in demonstrating the topological interface mode. In short, the exact zero modes in both the kinked and antikinked structures are topologically protected, while in a realistic single-waveguide input only the kinked structure can support such a robust interface mode due to the odd symmetry of its eigenmode. Our finding provides an indepth understanding of the dynamics of SPP defect modes within a well-defined waveguide array, and could cast new light on the optical simulations in condensed-matter physics and other photonic designs.

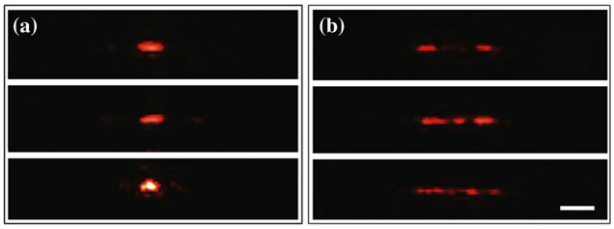

Figure 7 (a) Output intensities of three PWA-S1 samples with fabrication errors, which show almost unchanged localized field spots indicating robust SPP interface modes. (b) Output intensities of three PWA-S2 samples showing varied spreading features. Scale bar = 5 μm.

Supporting Information

Additional supporting information may be found in the online version of this article at the publisher's website.

Acknowledgements. The authors would like to thank B. G. Wang and H. Q. Wang for their helpful discussions. This work is supported by the National Key Projects for Basic Researches of China (No. 2012CB921501), the National Natural Science Foundation of China (Nos. 11174136, 11322439, 11321063, 91321312), the Dengfeng Project B of Nanjing University, and the PAPD of Jiangsu Higher Education Institutions.

Received: 15 December 2014, **Revised:** 25 May 2014, **Accepted:** 26 May 2014

Published online: 23 June 2014

Key words: Surface plasmon polariton, topological state, interface mode, optical waveguide.

References

[1] M. Z. Hasan, and C. L. Kane, Rev. Mod. Phys. **82**, 3045 (2010).
[2] X. L. Qi, and S. C. Zhang, Rev. Mod. Phys. **83**, 1057 (2011).
[3] S. Q. Shen, Topological Insulators Dirac Equation in Condensed Matters, (Springer, 2012).

[4] Z. Wang, Y. Chong, J. D. Joannopoulos, and M. Soljačić, Nature **461**, 772–775 (2009).
[5] M. Hafezi, S. Mittal, J. Fan, A. Migdall, and J. M. Taylor, Nature Photon. **7**, 1001–1005 (2013).
[6] M. C. Rechtsman, J. M. Zeuner, Y. Plotnik, Y. Lumer, D. Podolsky, F. Dreisow, S. Nolte, M. Segev, and A. Szameit, Nature **496**, 196–200 (2013).
[7] A. B. Khanikaev, S. H. Mousavi, W. K. Tse, M. Kargarian, A. H. MacDonald, and G. Shvets, Nature Mater. **12**, 233–239 (2013).
[8] K. Fang, Z. Yu, and S. Fan, Nature Photon. **6**, 782–787 (2012).
[9] W. Su, J. R. Schrieffer, and A. J. Heeger, Phys. Rev. Lett. **42**, 1698 (1979).
[10] J. Alicea, Rep. Prog. Phys. **75**, 076501 (2012).
[11] A. J. Heeger, S. Kivelson, J. R. Schrieffer, and W. P. Su, Rev. Mod. Phys. **60**, 781 (1988).
[12] M. Atala, M. Aidelsburger, J. T. Barreiro, D. Abanin, T. Kitagawa, E. Demler, and I. Bloch, Nature Phys. **9**, 795–800 (2013).
[13] J. M. Zeuner, M. C. Rechtsman, Y. Plotnik, Y. Lumer, M. S. Rudner, M. Segev, and A. Szameit, arXiv **1408**, 2191 (2014).
[14] T. Kitagawa, M. A. Broome, A. Fedrizzi, M. S. Rudner, E. Berg, I. Kassal, A. A. Guzik, E. Demler, and A. G. White, Nature Commun. **3**, 882 (2012).
[15] H. Schomerus, Opt. Lett. **38**, 1912 (2013).
[16] C. Poli, M. Bellec, U. Kuhl, F. Mortessagne, and H. Schomerus, arXiv **1407**, 3703 (2014).
[17] A. Poddubny, A. Miroshnichenko, A. Slobozhanyuk, and Y. Kivshar, ACS Photon. **1**, 101–105 (2014).
[18] D. N. Christodoulides, F. Lederer, and Y. Silberberg, Nature **424**, 817–823 (2003).
[19] I. L. Garanovich, S. Longhi, A. A. Sukhorukov, and Y. S. Kivshar, Physics Reports **518**, 1–79 (2012).
[20] Y. Xue, F. Ye, D. Mihalache, N. C. Panoiu, and X. Chen, Laser & Photon. Rev. **8**, L52–L57 (2014).
[21] Y. Liu, and X. Zhang, Appl. Phys. Lett. **103** 141101 (2013).
[22] E. Verhagen, R. Waele, L. Kuipers, and A. Polman, Phys. Rev. Lett. **105**, 223901 (2010).
[23] H. S. Eisenberg, Y. Silberberg, R. Morandotti, and J. S. Aitchison, Phys. Rev. Lett. **85**, 1863 (2000).
[24] A. Block, C. Etrich, T. Limboeck, F. Bleckmann, E. Soergel, C. Rockstuhl, and S. Linden, Nature Commun. **5**, 3843 (2014).
[25] N. Malkova, I. Hromada, X. Wang, G. Bryant, and Z. Chen, Opt. Lett. **34**, 1633–1635 (2009).
[26] S. H. Nam, E. U. Avila, G. Bartal, and X. Zhang, Opt. Exp. **18**, 25627–25632 (2010).
[27] S. Stafström, and K. A. Chao, Phys. Rev. B **29**, 2255 (1984); here, the sublattice symmetry is weakly broken because of the odd waveguide number $N = 79$ in PWAs.
[28] M. Golshani, S. Weimann, Kh. Jafari, M. Khazaei Nezhad, A. Langari, A. R. Bahrampour, T. Eichelkraut, S. M. Mahdavi, and A. Szameit, Phys. Rev. Lett. **113**, 123903 (2014).